J. Applied Membrane Science & Technology, Vol. 29, No. 3, December 2025, 271–289

Enhancing Superhydrophobic Polypropylene Membranes via Polypropylene Coating for Stable Membrane Distillation of Aquaculture Seawater

Siew Chun Low* & Jing Yi Chin

School of Chemical Engineering, Universiti Sains Malaysia,
14300 Nibong Tebal, Penang, Malaysia

Submitted: 12/9/2025. Revised edition: 24/10/2025. Accepted: 25/10/2025. Available online: 27/11/2025

ABSTRACT

Membrane distillation (MD) suffers from membrane wetting due to inadequate surface hydrophobicity, which limits long-term flux stability and desalination performance. Electrospun polypropylene (PP) membranes offer a promising solution because of their high porosity and interconnected fibrous structure that promote vapor transport. However, neat electrospun PP membranes often fall short of achieving the superhydrophobicity needed for durable wetting resistance, restricting their practical use in MD. To address this limitation, this study employed a dip-coating approach to deposit hydrophobic PP layers onto electrospun membranes, introducing a roughened surface that enhances hydrophobicity and mitigates wetting. Two coating formulations, i.e. low-viscosity (PP-L) and high-viscosity (PP-H), were examined. Morphological characterization revealed that PP-L coatings penetrated the membrane matrix, causing pore blockage and a severe flux decline (PPM-C3-L: 1.2 kg/m^2·h, 87.7% lower than neat PP). In contrast, PP-H coatings formed stereoscopic surface agglomerates without compromising porosity (82%) and achieving superhydrophobicity with a static contact angle of 156.7°. The optimal single-layer PP-H coated membrane (PPM-C1-H) maintained a high and stable flux of 13.3 kg/m^2·h for 25 h, with 99.98% salt rejection when treating aquaculture seawater. SEM–EDS analysis confirmed negligible scaling and no pore wetting despite the presence of $CaSO_4$, NaCl, and SiO_2 precursors in the feed. Overall, dip-coated PP-H surface offers a scalable approach to improve PP membranes for long-term, stable, and high-quality desalination of complex aquaculture effluents.

Keywords: Polypropylene, Membrane distillation, Water management, Superhydrophobic coating, Aquaculture seawater

1.0 INTRODUCTION

Water scarcity has become one of the most pressing global challenges, driven by population growth, industrialization, and climate change. Conventional desalination technologies such as reverse osmosis (RO) and multi-stage flash (MSF) distillation are already being deployed at large scale, but their application is hindered by high energy requirements, complex infrastructure, and susceptibility to fouling in high-salinity feeds. Membrane distillation (MD) has emerged as an attractive alternative, combining the benefits of thermal [1] and membrane-based processes. Unlike pressure-driven separations, MD relies on vapor transport through a hydrophobic membrane driven by a vapor pressure gradient, making it thermodynamically capable of achieving nearly complete salt

* Corresponding to Siew Chun Low (email: chsclow@usm.my)
DOI: https://doi.org/10.11113/jamst.v29n3.327

rejection while tolerating high salinity levels [2]. Its relatively low operating pressure and compatibility with low-grade or waste heat sources further underscore its potential for sustainable water production [3]. Nevertheless, the successful application of MD critically depends on the development of membranes with optimized structural and surface properties.

The key requirement for MD membranes is hydrophobicity, as it prevents liquid water from intruding into the pores while allowing only vapor transport. Conventional commercial membranes, such as those fabricated from polytetrafluoroethylene (PTFE), polyvinylidene fluoride (PVDF), and polypropylene (PP), exhibit moderate hydrophobicity [4] but often fail under prolonged exposure to high temperatures, high salinities, or complex wastewater compositions. Numerous strategies have been proposed to enhance membrane hydrophobicity and wetting resistance, including electrospinning [5], plasma-grafting [6], and nanocomposite incorporation [7]. For instance, electrospun nanofibrous structures are valued for their high porosity and tunable surface roughness, which improve the stability of the air–water interface. Similarly, plasma-induced fluorination or the deposition of nanoparticles such as silica or TiO_2 has been reported to impart superhydrophobicity [8]. However, such approaches frequently involve high fabrication costs, complicated processing, or incorporation of foreign additives that may compromise long-term chemical stability. A scalable and material-compatible method of modifying membrane surfaces while maintaining their intrinsic advantages is therefore highly desirable.

The tolerance of MD to high-salinity and complex wastewater streams distinguishes it from pressure-driven desalination technologies. In particular, MD is capable of processing hypersaline brines that are beyond the operational limits of RO, thereby enabling more sustainable water cycles. This feature makes MD particularly relevant to seawater desalination and industrial brine management. More recently, its potential has been explored in aquaculture wastewater treatment [9,10], where the effluents are not only saline but also enriched with nutrients, organic matter, and chemical residues. These constituents accelerate fouling and scaling in conventional membrane processes, reducing flux and lifespan. In contrast, the thermally driven nature of MD diminishes the impact of these contaminants, and elevated feed-temperature can inhibit microbial growth. Demonstrating MD performance in treating aquaculture wastewater thus represents a promising but underexplored application space, where robust membrane design is critical to maintaining high flux and salt rejection under challenging operating conditions.

Among the available membrane materials, polypropylene (PP) stands out as a promising candidate for MD due to its inherent hydrophobicity, chemical resistance, and cost-effectiveness. PP has been widely used in commercial hollow-fiber modules [11] and electrospun membranes [12], with studies demonstrating its suitability for desalination and wastewater treatment. Electrospun membranes, in particular, offer interconnected porous networks and rough surface morphologies that enhance hydrophobic behavior [13–15]. Yet, neat electrospun PP often falls short of achieving the superhydrophobicity required for robust wetting resistance in long-term operation. Coating strategies that use

PP itself as the surface-modifying agent offer an attractive solution, as they preserve material compatibility, avoid introducing foreign additives, and leverage PP's semicrystalline structure to tune surface topography [16]. Nonetheless, systematic investigations on how the viscosity of PP coating dopes influence surface crystallization, agglomerate formation, and overall MD performance remain scarce.

This work addresses this critical research gap by developing superhydrophobic PP membranes through electrospinning followed by surface coating with PP solutions of different viscosities. Unlike conventional approaches that rely on fluorination or inorganic nanoparticles, our method exploits the intrinsic molecular characteristics of PP to achieve surface modification without compromising chemical compatibility. We hypothesize that PP solutions of different viscosities, reflecting variations in polymer chain length and entanglement, will lead to distinct crystallization behaviors and morphological outcomes on the membrane surface. By systematically comparing high-viscosity and low-viscosity PP coatings, we demonstrate how polymer chain interactions govern surface agglomeration, porosity retention, and hydrophobic enhancement. Furthermore, the modified membranes are evaluated for their performance in direct contact membrane distillation (DCMD) using both saline water and real aquaculture effluents. The main novelty of this work lies in establishing a simple yet effective PP-on-PP coating strategy that produces durable superhydrophobic membranes while avoiding foreign additives. The study not only elucidates the structural mechanisms underlying viscosity-controlled coating but also validates the practicality of the best-performing membranes for treating challenging high-salinity and nutrient-rich wastewater streams. By bridging material-level innovation with application-level validation, this work contributes both fundamental insights and a scalable pathway toward advancing MD for sustainable desalination and aquaculture wastewater management.

2.0 METHODS

2.1 Chemicals or Materials

Electrospun polypropylene (PP) membrane with an average pore size of 10 μm was obtained from Sterlitech (USA). Polypropylene (PP) pellets supplied by Lotte Chemical Titan (Malaysia) were used to prepare the coating solution. The coating chemicals, including xylene and methyl ethyl ketone (MEK) were supplied by Sigma-Aldrich and Merck, respectively.

2.2 Surface Modification on the Electrospun Membrane

High-viscosity (PP-H) and low-viscosity (PP-L) polypropylene (PP) polymers were used as coating dopes to modify the neat PP membrane. Before preparing the dope solutions, both PP grades were dried overnight in an oven at 70 °C to remove residual moisture. The dope was then prepared by dissolving granulated PP in xylene at 120 °C using a silicon oil bath, with continuous stirring at 350 rpm for 1 h until the polymer was fully dissolved.

Membrane coating was performed using a manual dip-coating approach. During dope preparation, neat PP membranes were fixed horizontally on stainless-steel holders with binder clips (Figure 1). Two stainless-steel

containers were prepared: one filled with methyl ethyl ketone (MEK) and the other with PP dope solution, which was maintained at 90 °C to ensure a uniform coating temperature across all samples. Each neat PP membrane was first immersed in MEK for 30 s and subsequently dipped into the PP dope for 10 s. MEK acts as a surface-conditioning agent that mildly swells the PP membrane, enhancing coating adhesion and uniformity during the subsequent PP dip-coating step.

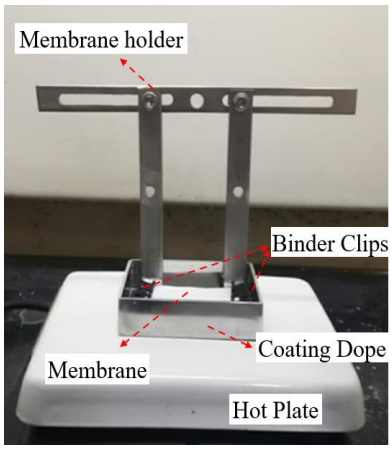

Figure 1 Dip-coating set-up

The membrane was fully submerged in the dope, and the holder was gently shaken in a biaxial manner to promote even deposition of PP on the surface. Coated membranes were then placed in a vacuum oven (70 °C, around 0.33 Pa) to control the solidification rate and prevent heterogeneous PP oxidation. The membranes were dried for 1 h until the coated layer turned white, indicating complete solidification. In this study, triple-layer coating was also performed for comparison with the single-layer coating. Before DCMD performance tests, the membranes were manually separated into bilayers. The PP-coated surface was then oriented toward the hot feed side, while the uncoated surface faced the cold permeate side. The rationale for this membrane splitting is further explained in the Results and Discussion section.

Surface and cross-sectional morphologies of the coated membranes were examined by SEM. Hydrophobicity was assessed via static water contact angle measurements. Porosity of neat and coated membranes was determined using the 2-butanol uptake method: 1 cm × 2 cm membrane strips were immersed in 2-butanol for 2 h, weighed in the wet state, then dried in an oven and reweighed. Porosity was calculated using the equation reported in previous work [17]. Membrane thickness was measured using a Mitutoyo thickness gauge, which was calibrated to zero prior to measurements. Thickness was determined at multiple spots across each membrane to obtain average values.

2.3 Evaluation of the Membrane Performances

Direct contact membrane distillation (DCMD) was employed to evaluate the separation performance of both neat and coated membranes, and a similar setup can be found in our previously published work [17]. A transparent membrane module with an effective area of 0.00085 m^2 was used. The module consisted of two compartments, where the hot and cold streams were circulated in cross-flow configuration on opposite sides of the membrane. A microporous support was placed on the cold side to provide mechanical stability during DCMD operation. For each test, the coated surface of the membrane was oriented towards the hot feed. All DCMD experiments were conducted with the hot feed maintained at 60 °C and the cold permeate stream at 20 °C. Both streams were circulated at a flow rate of 0.3 L/min. The mass of permeate

collected was recorded at 5 min intervals, and the permeate flux (J, $kg/m^2 \cdot h$) was calculated according to Eq. 1.

$$J = \Delta m/A.\Delta t \quad (1)$$

where Δm (kg) is the mass of water transported from the hot feed to the cold permeate during the time interval Δt (h), and A (m^2) is the effective membrane area. DCMD runs were performed over short-term (2 h) and long-term (25 h and 60 h) durations. For short-term tests, the conductivity of permeate (Cp) was measured every 15 min, while for long-term runs, measurements were taken hourly using a conductivity meter. Salt rejection (R, %) was determined using Eq. 2.

$$R = (1-C_p/C_f)\times 100\% \quad (2)$$

where C_p is the conductivity of the permeate and C_f is the conductivity of the hot feed solution.

2.4 Hot feed for DCMD Separation Tests

Two different water sources were used as the DCMD hot feed: synthetic high-salinity water and fish farm seawater. To mimic the salinity of aquaculture effluent, a 35 g/L NaCl solution prepared with deionized (DI) water was used as the synthetic saline feed for screening the performance of coated membranes. The best-performing coated membrane identified in this step was subsequently evaluated for its ability to purify actual fish farm seawater. The fish farm seawater was collected from open waters in the Straits of Malacca, near the Penang Second Bridge, Malaysia. Sampling was carried out at a water depth of 4-5 m, with surface water collected for testing. Prior to use as the DCMD hot feed, the seawater was vacuum-filtered to remove suspended solids. The composition of both the raw seawater and the DCMD cold permeate was analyzed to assess the membrane's effectiveness in preventing the passage of undesirable constituents.

Organic species (NO_3^-, NO_2^-, and NH_3) and inorganic species (PO_4^{3-}, SiO_2, and Cl^-) in both feed and permeate were quantified using a portable photometer (Lovibond Maxi Direct, Tintometer). For each analysis, the photometer was calibrated to zero with a blank sample before measurement. Test-specific reagents were then added, and the resulting concentrations were determined photometrically. Concentrations of Na, Ca, and Mg were measured using atomic absorption spectrometry (AAS) with an air–acetylene flame, at wavelengths of 589.0, 422.7, and 285.2 nm, respectively. All measurements were performed in triplicate, and average values were reported.

3.0 RESULTS AND DISCUSSION

Due to the inherently hydrophobic nature of polypropylene (PP) and the rough surface created by the crisscrossed nanofibers during the electrospinning process, the neat electrospun PP membrane exhibits hydrophobicity, with a static water contact angle of 138.0 ± 3.6°. Nevertheless, this value does not yet qualify as superhydrophobic. To further enhance its hydrophobicity, a thin coating of PP was applied onto the surface of the electrospun membrane. Two types of PP polymers were used as coating solutions: one with relatively high viscosity (PP-H, 10.53 ± 2.0 cP) and the other with low viscosity (PP-L, 3.22 ± 0.2 cP). Since higher viscosity typically reflects longer polymer chains, the PP-H

solution is expected to undergo stronger molecular chain entanglements compared with PP-L. This difference in chain interactions is likely to influence their crystallization behavior and, consequently, the morphological characteristics of the coated membranes.

Prior to applying the coating on the pristine membrane, the functional groups of both PP dopes and the pristine PP membrane were characterized using FTIR (Figure 2). The spectra revealed that all samples displayed peaks within the same wavenumber ranges, suggesting that the dopes and the neat membrane share identical elemental compositions. Specifically, characteristic absorption bands were observed at 2952, 2919, and 2839 cm^{-1}, corresponding to C–H stretching vibrations. The peaks at 2952 and 2839 cm^{-1} are assigned to CH_3 asymmetric stretching, while the 2919 cm^{-1} band corresponds to $–CH_2–$ symmetric stretching. The peak at 1454 cm^{-1} indicates $–CH_2–$ symmetric bending, and the 1378 cm^{-1} peak is attributed to symmetric bending of the methyl group. Consecutive peaks at 1165, 997, and 973 cm^{-1} are associated with $–CH_3$ rocking vibrations; additionally, the 997 and 973 cm^{-1} bands also correspond to C–C stretching, representing the polymer backbone of PP [18]. Furthermore, absorption bands at 1165, 997, and 840 cm^{-1} are characteristic of crystalline PP, while peaks at 1378 and 973 cm^{-1} reflect contributions from both crystalline and amorphous regions [19]. Collectively, these observations confirm the semicrystalline nature of PP.

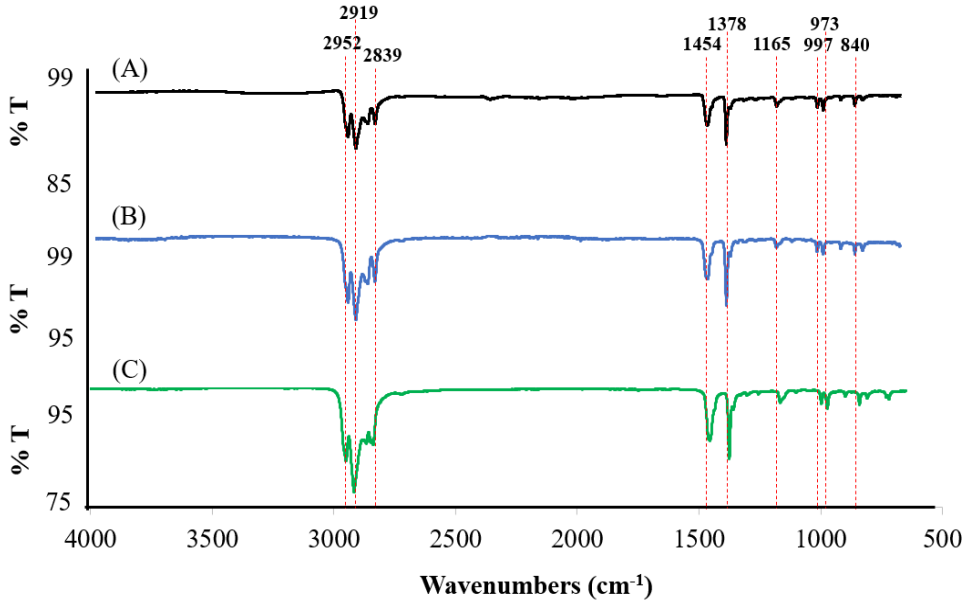

Figure 2 FTIR fingerprint region of (A) pristine polypropylene membrane (PPM-C0), and polypropylene coating dope with (B) high viscosity (PP-H) and (C) low viscosity (PP-L)

The pristine membrane was first evaluated to establish a benchmark for DCMD performance. After a 2-hour separation test, the membranes were removed from the DCMD module. Unexpectedly, the originally intact membrane was found to have liquid trapped inside, forming an air–water pocket as shown in Figure 3A. Interestingly, the two membrane layers that faced opposite feed solutions exhibited different physical appearances. The layer in contact with the cold feed (Figure 3B-left) retained

its original flat conformation, while the layer exposed to the hot feed (Figure 3B-right) showed visible swelling. This observation (Figure 3B) suggests that the membrane is unsuitable for effective separation. To further probe this behavior, the membrane was manually split into two distinct layers. As anticipated, the layers could be separated with ease, indicating that the bilayer structure was not firmly bonded. During DCMD operation, the two layers experienced opposing thermal environments (Figure 3C): the surface facing the hot feed softened and expanded due to elevated temperature, while the surface in contact with the cold feed remained comparatively rigid. Moreover, the temperature gradient across the hot-side layer was uneven, with the outer surface (ho) experiencing greater expansion than the inner surface (hi). This imbalance promoted outward bending and partial delamination from the cold-side layer, thereby creating interlayer voids. Within these voids, vapor originating from the hot feed could lose kinetic energy upon direct contact with the cold-side layer, resulting in premature condensation into water droplets. This increased the effective diffusion path and raised the likelihood of condensation before vapor could traverse the intact cold-side layer. While some vapor successfully passed through and contributed to permeate flux, a significant fraction condensed within the delaminated regions. The accumulation of liquid further expanded the air–water pocket, amplifying mass transfer resistance and severely diminishing flux performance.

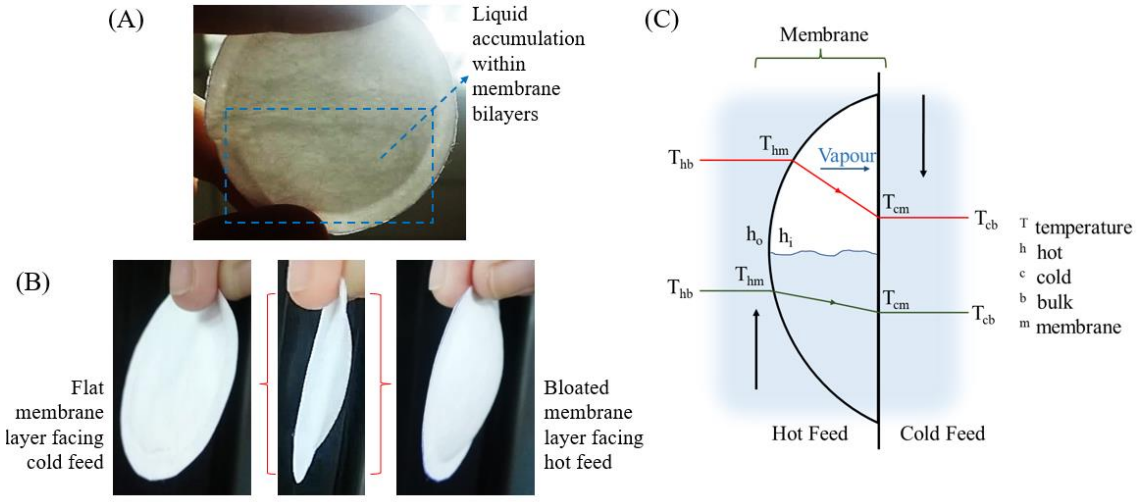

Figure 3 (A) Post DCMD membrane condition whereby liquid trapped within bilayers PPM-C0 (B) Schematic illustration of temperature gradient across air/water trapped membrane while performing DCMD test

Because liquid entrapment within the membrane during DCMD operation compromises both permeate flux and process stability, all membranes in subsequent experiments were manually split prior to characterization and DCMD testing. The thicknesses of single- and triple-layer PP-L and PP-H coated membranes were measured and are summarized in Table 1. The observed increase in thickness confirmed that

both PP-L and PP-H were successfully deposited onto the neat PP membrane. During the multilayer coating process, the underlying coated layers were partially melted upon contact with the hot PP dope containing xylene, which induced a reorganization of the crystalline structure within these layers. The sequential stacking of coatings also restricted the available space for spherulite formation in the lower layers. As a result, PP lamellae tended to grow parallel to the interface, forming flattened or discoid spherulites [20]. This structural rearrangement explains the non-linear increase in thickness with successive coatings. Overall, PP-H coated membranes exhibited greater thickness compared to PP-L coated membranes. This observation is consistent with the explanation by Baig *et al*. [21], who reported that high-viscosity polymer solutions slow down solvent exchange rates. The delayed solvent–polymer demixing process favors the formation of larger, unevenly distributed PP-H agglomerates, which protrude and contribute to the development of a thicker polymer layer.

Table 1 Thickness of membranes coated with PP-L and PP-H dopes

Membrane ID	Thickness (mm)	% increment of thickness
PPM-C0	0.092 ± 0.008	-
PPM-C1-L	0.111 ± 0.007	20.7
PPM-C3-L	0.143 ± 0.009	55.4
PPM-C1-H	0.123 ± 0.016	33.8
PPM-C3-H	0.178 ± 0.029	92.3

Figure 4 presents the surface morphologies of both sides of the PP membranes. The uncoated inner surface was designed to face the cold permeate, while the outer surface, coated with either PP-L or PP-H dopes, served as the hydrophobic layer exposed to the hot feed. For the neat membrane (PPM-C0), both sides exhibited similar morphologies. Likewise, the inner surface of the single-layer coated PPM-C1-L resembled that of PPM-C0, with no evidence of significant penetration of the PP-L dope into the membrane matrix. In contrast, the inner surface of the triple-layer coated PPM-C3-L clearly revealed deep infiltration of PP-L into the cross-section of the membrane, with polymer brushes observed along the nanofiber walls. This phenomenon raises concern, as excessive polymer intrusion can reduce the membrane's internal void space, which is crucial in MD applications for minimizing conductive heat loss and lowering vapor mass transfer resistance [22]. On the other hand, SEM images of PPM-C1-H and PPM-C3-H showed clean inner surfaces with no visible penetration of PP-H into the membrane structure (Figure 4). Consistent with this observation, porosity measurements demonstrated that the neat membrane (PPM-C0) had a bulk porosity of 74.5 ± 1.0%, while PPM-C1-H and PPM-C3-H maintained similar porosities of 75.7 ± 2.8% and 73.0 ± 4.5%, respectively. These findings suggest that surface coatings with PP-H do not compromise membrane porosity. Likewise, PPM-C1-L and PPM-C3-L exhibited similar porosities of 74.3 ± 1.4% and 71.2 ± 3.5%, respectively, confirming that the coating process preserved the overall porous structure. Therefore, the impact on vapor mass transfer resistance is expected to remain minimal following PP modification.

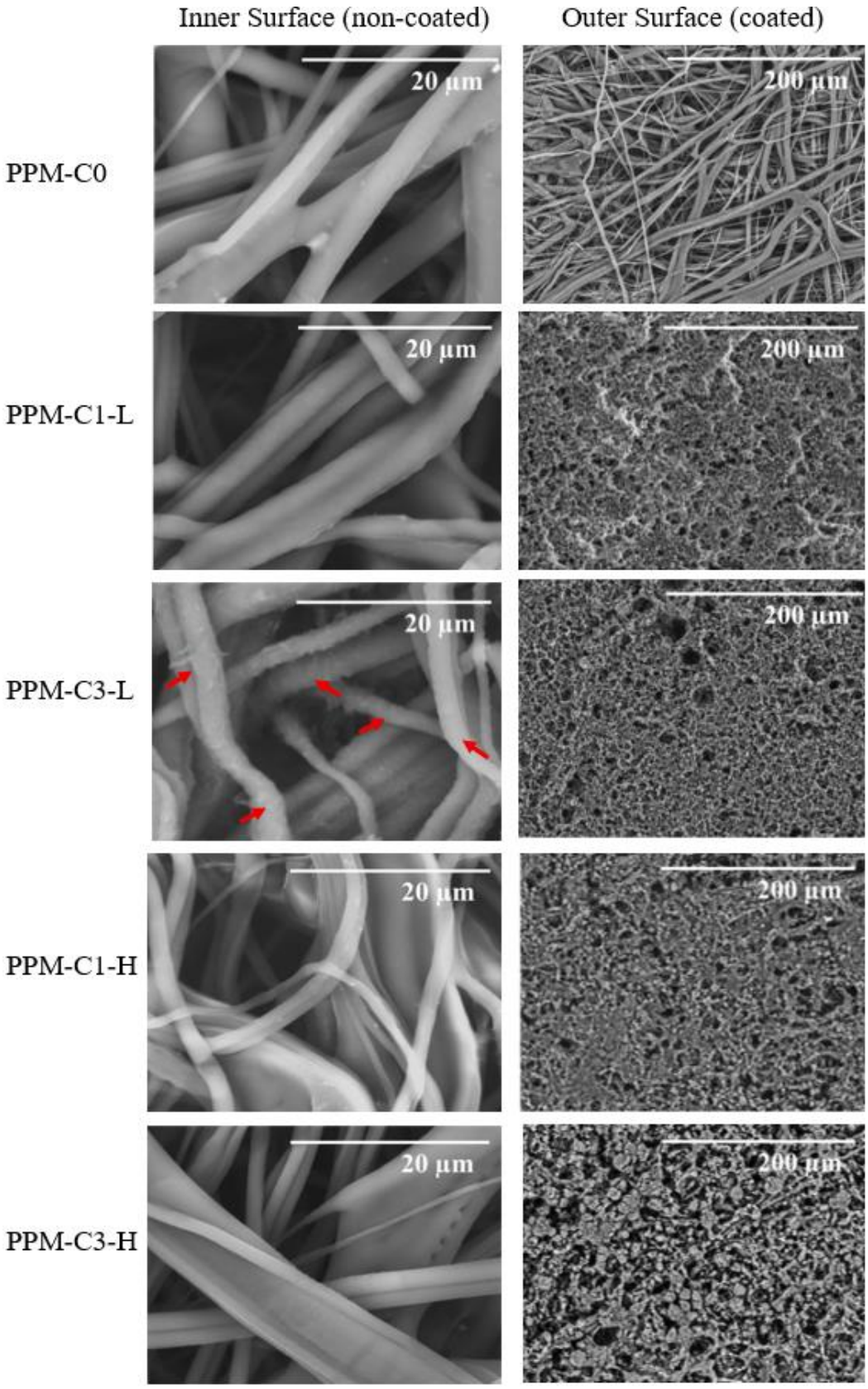

Figure 4 SEM micrographs of inner uncoated surface (DCMD cold permeate) and outer coated surface (DCMD hot feed) of membranes at different layers and viscosity grade of polypropylene solutions

Turning to the outer surfaces of the PP-coated membranes (Figure 4, right images), the micrographs revealed the presence of PP agglomerates distributed across the surface. The formation of these surface layers requires PP chains to undergo cycles of disentanglement and re-entanglement. For both PP-L and PP-H coatings, the compactness of PP clusters increased with additional coating layers, indicating a progressive buildup of deposited material. This stacking process suggests that recrystallization occurred during coating. Specifically, melted lamellae on the coated surface acted as self-seeds, giving rise to new nuclei, which subsequently grew into thicker lamellae. As these lamellae expanded, PP agglomerates accumulated and fused together [23]. Notably, under the same number of coating layers, the surfaces of PPM-C1-H and PPM-C3-H displayed more stereoscopic and spatially separated agglomerates compared with their PP-L counterparts. This behavior can be attributed to the stronger intermolecular interactions among the longer PP-H chains, both across multilayers and within individual layers. These interactions are primarily governed by forces between hydrogen atoms. The enhanced chain interactions in PP-H coatings promote crystal growth into distinct globules[24], where the lamellae are pulled apart as they pack more densely within their respective domains.

Contact angle measurements were conducted to verify the surface morphology observed by SEM. The PPM-C1-H membrane exhibited superhydrophobicity with a contact angle of 156.7 ± 3.8°, confirming the effectiveness of the surface modification. However, after three coating layers, PPM-C3-H showed a lower contact angle of 147.8 ± 3.0°, likely due to the formation of a more compact PP coating structure, as observed in Figure 4. In contrast, the lower-viscosity PP-L formed a thinner coating layer on the membrane surface (Table 1), resulting in lower contact angles of 149.5 ± 2.5° and 144.6 ± 2.7° for PPM-C1-L and PPM-C3-L, respectively.

Figure 5 summarizes the membrane performances in converting a 35 g/L salt solution into pure water. The average flux of PPM-C1-L was 10.4 kg/m²·h, which was comparable to that of the neat membrane, PPM-C0 (9.8 kg/m²·h). This similarity in flux supports the earlier observation (Figure 4, PPM-C1-L) that no significant penetration of PP-L dope occurred during the single-layer coating. In contrast, PPM-C3-L exhibited a drastic flux reduction of 87.7%, yielding only 1.2 kg/m^2·h. This decline can be attributed to the combined effects of coating dope penetration and increased membrane thickness. Such penetration is typical for low-viscosity polymers with shorter chains, as they tend to infiltrate deeper into the substrate during coating [25], consistent with the SEM findings for PPM-C3-L (Figure 4, left). Although PPM-C3-L maintained excellent salt rejection (>99.99%), its severely reduced flux indicates that surface modification with PP-L is not effective when compared to the neat membrane, which also achieved near-complete salt rejection. In contrast, membranes coated with PP-H displayed superior performance. Both PPM-C1-H and PPM-C3-H achieved higher fluxes than PPM-C0, highlighting PP-H as the more suitable dope for superhydrophobic surface modification. PPM-C1-H achieved the highest flux of 13.0 kg/m^2·h, while PPM-C3-H recorded a slightly lower value of 11.0 kg/m^2·h. The flux enhancement can be attributed to the significant improvement in membrane

hydrophobicity. By elevating the air–liquid interface to the membrane surface, a larger dry region was created between the flowing feed water and the membrane, thereby facilitating vaporization and improving flux throughput [17,26]. Overall, these results demonstrate that PP-H is more effective than PP-L in modifying membrane surface topography to enhance flux while maintaining salt rejection consistently above 99.99% throughout the desalination process.

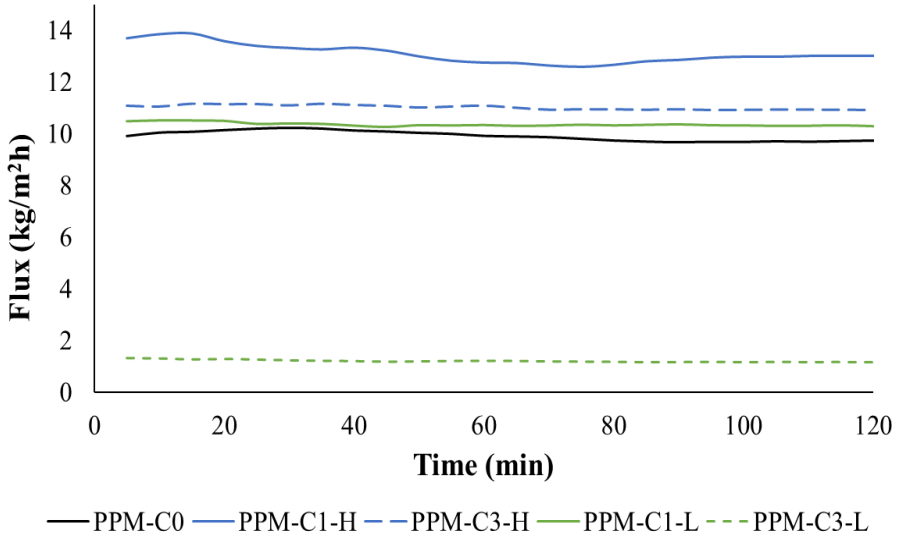

Figure 5 DCMD flux of membranes coated with different layers and viscosity grade of polypropylene solutions

The rapid expansion of aquaculture activities has created an urgent need to treat wastewater, both to reduce its environmental impact and to enable potential reuse. Although not yet widely applied, MD shows promise as a treatment technology for aquaculture effluents. Unlike pressure-driven membrane processes, MD performance is less sensitive to the complex mixture of constituents typically found in wastewater, making it a feasible option for this application. In this study, particular focus was placed on evaluating the viability of MD and, more importantly, the practicality of using surface-modified membranes, especially the best-performing PPM-C1-H, for treating seawater from offshore fish farms. The composition of fish farm seawater is inherently complex (Table 2). In addition to the baseline salinity and minerals naturally present in seawater (pH 7.55 in this study), aquaculture effluent contributes significant amounts of waste. Nitrogen (N) and phosphorus (P) are the principal components of fish feed, which is formulated with high crude protein content. However, fish are able to assimilate less than 50% of the nutrients consumed, while the remainder is released into the culture water [27]. Moreover, fecal matter and excretory products from fish also contain N and P, ranging widely from 1% to 70%. Excess N and P in aquaculture waters can exert toxic effects on fish health, making their removal essential. In this study, the concentrations of N and P in the sampled seawater were not significantly elevated, likely due to dilution effects in the open-water system. Beyond nutrients, aquaculture waters may contain trace levels of

chemicals, such as medications, disinfectants, and antifoulants, used to maintain fish health, despite their regulated and restricted application. These substances, together with nutrient residues, represent potential foulants that could contribute to scaling or fouling of MD membranes during operation.

Table 2 Concentrations of components in DCMD feed (fish farm water) and permeate and their respective rejection rate

Components	Unit	Feed	Permeate	Malaysia Drinking Water Standard	Rejection (%)
Nitrate, NO_3	mg/L	< 4.0	< 4.0	10	-
Nitrite, NO_2	mg/L	0.09	< 0.03	-	-
Phosphate, PO_4	mg/L	0.15	< 0.06	-	-
Ammonia, NH_3	mg/L	4.85	0.12	1.5	97.52
Silica, SiO_2	mg/L	0.39	0.09	-	76.92
Chloride, Cl^-	mg/L	35040	140	250	99.60
Sodium, Na	mg/L	10920.30	4.30	200	99.96
Magnesium, Mg	mg/L	1150	0	150	100
Calcium, Ca	mg/L	567.20	0.10	-	99.98

The permeate flux obtained from MD using the PPM-C1-H membrane to treat fish farm seawater is presented in Figure 6. The average clean water production rate was 13.3 kg/m²·h over a continuous 25-hour operation, which is comparable to the flux achieved with the pure NaCl solution (Figure 5). Given the complex composition of aquaculture seawater, the membrane in the DCMD system is potentially vulnerable to various fouling mechanisms, including inorganic salt scaling, biofouling, and chemical degradation [9]. Remarkably, as shown in Figure 6, the flux profile remained stable, with only minimal fluctuations, indicating the absence of significant foulant deposition that could impair performance. In addition, liquid intrusion into the membrane pores was negligible, as evidenced by the consistently high salt rejection of 99.98%.

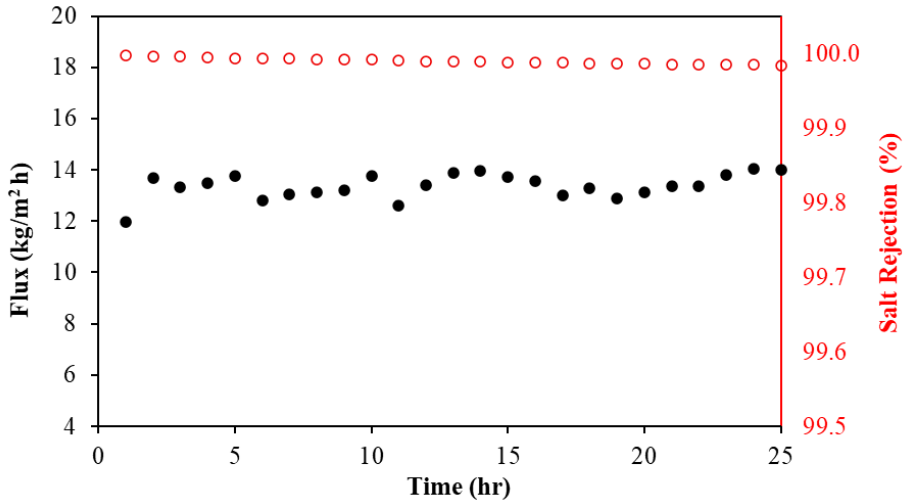

Figure 6 Flux and salt rejection performance of PPM-C1-H in purifying fish farm seawater employing DCMD

In addition to the robustness of the PPM-C1-H membrane against foulant attachment, the elevated feed temperature in MD also contributed to reducing fouling, particularly biological fouling. Microbial growth, which is commonly encountered in seawater treatment processes, is strongly inhibited under high-temperature conditions. As a result, the likelihood of microorganisms blocking membrane pores and obstructing vapor diffusion was minimal [28,29]. The practicality of the PPM-C1-H membrane was further validated through an assessment of permeate quality. As summarized in Table 2, the concentrations of all analyzed components in the permeate were markedly lower than in the feed solution. With the exception of silica, rejection rates for all constituents exceeded 97%, demonstrating the excellent retention capability of the membrane. The lower rejection of silica can be explained by its behavior at elevated temperatures: SiO_2 dissolves into the feed water as monosilicic acid, which may infiltrate the membrane sublayer and promote scaling along pore walls [30]. When benchmarked against Malaysia's drinking water standards, the permeate quality from fish farm seawater treatment was exemplary, with all measured parameters falling well below the permissible limits. These results confirm that coupling MD with PPM-C1-H membranes not only mitigates the environmental impact of aquaculture wastewater but also produces purified water of sufficient quality for potential reuse.

As the feed components were effectively rejected by the membrane, the DCMD feed was expected to become progressively concentrated during the separation process. To gain further insight into the interactions between these retained components and the membrane, SEM-EDS analyses were carried out on both the surface and cross-section of the PPM-C1-H membrane after DCMD operation (Figures 7 and 8).

After 25 hours of continuous operation, the membrane showed no significant signs of abrasion, as the PP agglomeration layer on PPM-C1-H remained intact, as confirmed by the FESEM micrograph in Figure 7. Importantly, no substantial deposition of salt crystals was detected on the membrane surface. The EDS spectrum (Figure 7) revealed a strong carbon peak, primarily reflecting the membrane's intrinsic composition, with a minor contribution possibly from carbonate residues. In contrast, signals from other elements originating from the aquaculture seawater appeared only as very weak peaks.

Although relatively minor, sporadic deposits were still observed on the membrane surface after DCMD, as shown by the EDS mapping in Figure 7. The elemental distribution suggests the presence of NaCl and $CaSO_4$ precipitates, since Na and Cl appeared in overlapping regions, as did Ca, S, and O. Other salt crystals may also have formed on the surface, given the complex molecular interactions occurring on the feed side during aquaculture seawater purification. Importantly, both $CaSO_4$ and NaCl deposits were largely confined to the surface, as their concentrations within the membrane cross-section were minimal, as confirmed by EDS line scans (Figure 8). The two salts, however, behave differently at elevated temperatures. NaCl, which has higher solubility at elevated temperature, is generally less prone to crystallization during desalination. Still, the naturally high concentrations of Na and Cl in seawater (Table 2) make it easy to reach supersaturation, leading to NaCl crystal formation. Moreover, NaCl is

well known to crystallize readily on membrane surfaces upon drying [31]. In this study, the observed NaCl deposition on the PPM-C1-H membrane may also have resulted from this effect, since the membrane was dried with residual fish farm seawater prior to FESEM-EDS analysis.

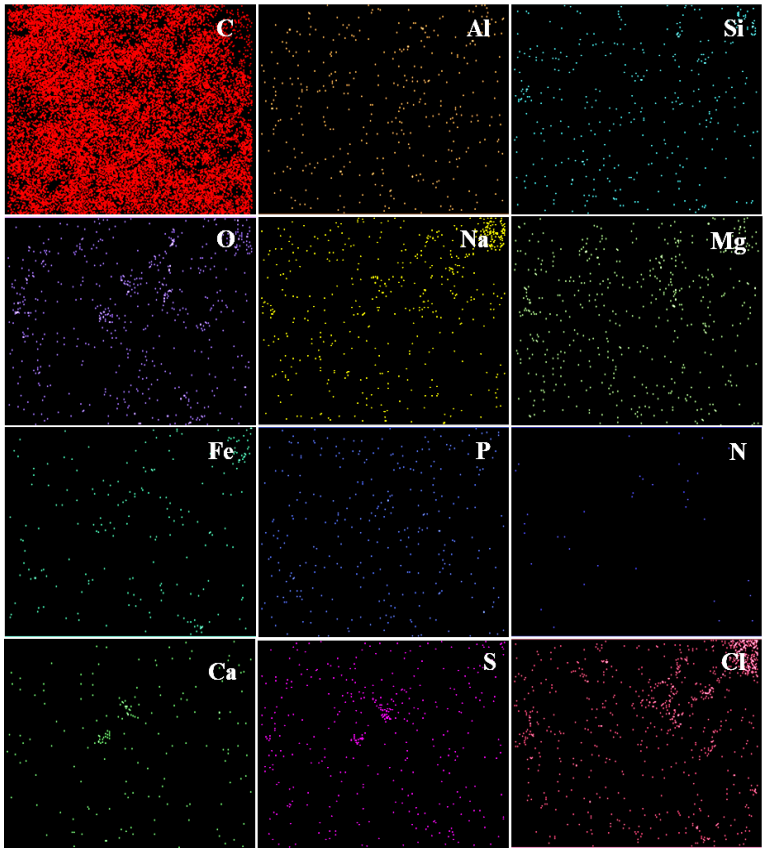

Figure 7 FESEM-EDS mapping of components presents on PPM-C1-H surface after fish farm water treatment in DCMD

Compared with NaCl, $CaSO_4$ is a non-alkaline salt that exhibits retrograde solubility at temperatures above 50 °C [32]. Another calcium salt with inverse solubility behavior is $CaCO_3$. Although typically present at lower concentrations than $CaSO_4$, $CaCO_3$ can also contribute to membrane scaling during seawater desalination [33]. Studies with single-salt solutions indicate that $CaCO_3$ precipitates rapidly, while $CaSO_4$ requires a longer induction time before crystallization occurs. However, when both salts are present, their scaling behavior changes significantly, where a non-dominant concentration of $CaCO_3$ can markedly influence the thermodynamics and kinetics of $CaSO_4$ precipitation [34]. Specifically, co-precipitation of the two salts began almost immediately, eliminating the induction time observed in single-salt systems. Moreover, $CaCO_3$ was found to consolidate the initially loose $CaSO_4$ deposits, forming a more compact and adherent scale. This explain why $CaSO_4$ tended to dominate the scaling behavior in this co-precipitation system.

The EDS line scan of the PPM-C1-H cross-section (Figure 8) provides further insight into potential scaling within the membrane. Across the

membrane thickness, the signal intensities of all analyzed elements were very low, with the exception of carbon, which reflects the PP backbone structure. This observation supports the conclusion that membrane wetting was negligible during treatment of fish farm seawater. Interestingly, a sharp increase in elemental signals was detected at a depth of around 60 µm, particularly for silicon. Since silicon commonly occurs as SiO_2 in scaling deposits, this rise suggests localized accumulation. In membrane-based separations, SiO_2 is especially problematic because of its strong tendency to block pores rather than form a surface layer [33]. Similar to NaCl, dissolved silica in heated solutions do not easily precipitate unless other species are present. However, trace amounts of Al, Fe, and Mg can significantly accelerate silica precipitation. For instance, SiO_2 readily adsorbs onto Fe(III) hydroxide colloids, which can serve as nucleation sites for silica and aluminosilicate formation. Meanwhile, Mg salts promote deposition of both colloidal and monomeric silica within membrane structures [35].

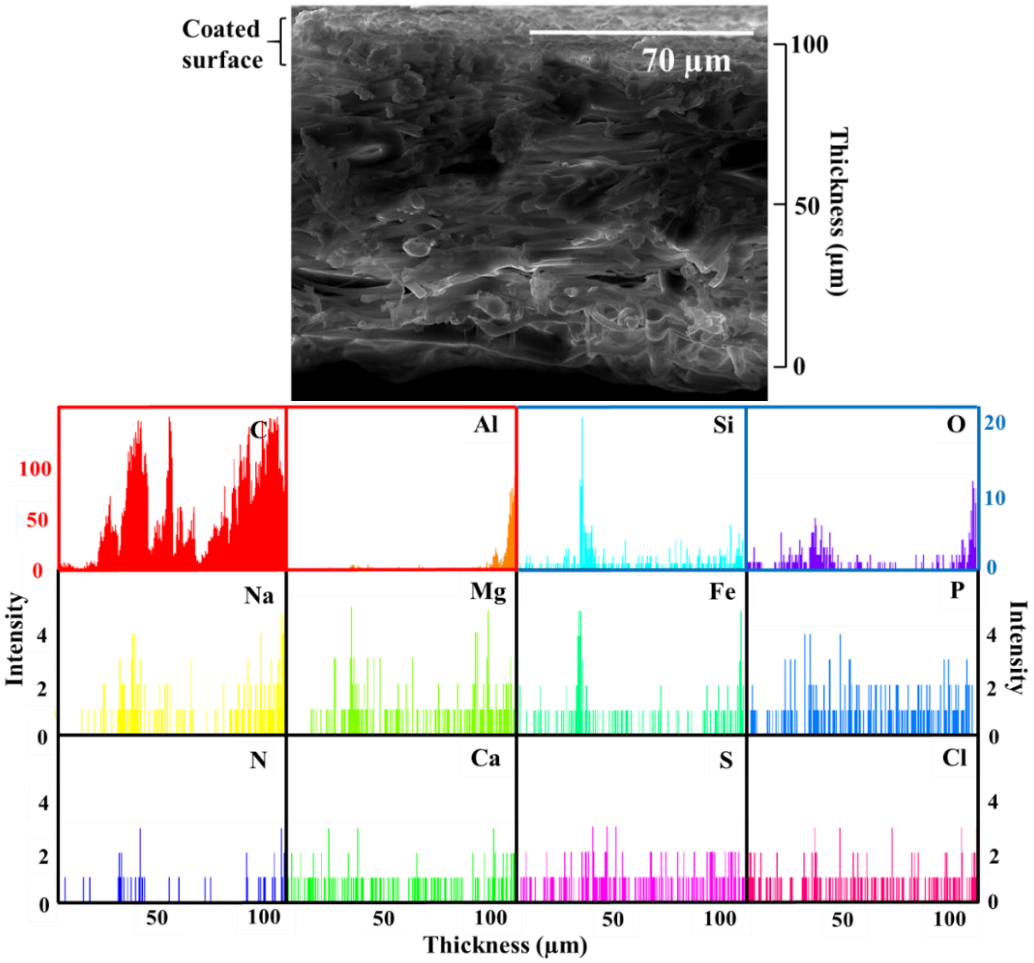

Figure 8 FESEM-EDS lining of components presents n PPM-C1-H cross-section after fish farm water treatment in DCMD

Considering the overall elemental intensity profile of PPM-C1-H, the consistently low signals near the membrane surface suggest that the sharp peaks observed deeper within the cross-section are unlikely to originate

from foulant intrusion. Instead, these peaks may be attributed to artifacts introduced during drying or minor cracking of the membrane. Overall, the presence of foulants on both the surface and within the cross-section of PPM-C1-H was negligible and did not affect DCMD flux, either qualitatively or quantitatively. This favorable performance can be attributed to the superhydrophobic nature of the S-PP/6331-L1 coating. The nanoscale roughness of the PPM-C1-H surface helps sustain a stable air layer, effectively reducing direct liquid–membrane contact. As a result, potential nucleation sites for inorganic scaling are minimized. Furthermore, any loosely attached foulants or scalants that temporarily accumulate at the liquid–air interface are likely swept away by the cross-flowing feed solution [36]. This mechanism not only limits surface deposition but also reduces the risk of pore wetting caused by fouling or scaling.

4.0 CONCLUSION

This study demonstrated that coating polypropylene membranes with high-viscosity PP (PP-H) effectively enhanced surface hydrophobicity and DCMD performance. Unlike PP-L coatings that penetrated and blocked pores, PP-H coatings preserved porosity (82%) and achieved superhydrophobicity (156.7°). The optimized PPM-C1-H membrane delivered stable flux of 13.3 $kg/m^2 \cdot h$ for 25 h, with near-complete salt rejection (99.98%) when treating aquaculture seawater. SEM–EDS confirmed negligible scaling or fouling, even in the presence of $CaSO_4$, NaCl, and SiO_2 precursors. Overall, PP-H coatings provided a scalable modification strategy, enabling long-term desalination with stable flux and high-water quality, while minimizing risks of fouling and wetting.

ACKNOWLEDGEMENT

Special thanks to Universiti Sains Malaysia for the financial assistance through Bridging Grant (R501-LR-RND003-0000002171-0000).

CONFLICTS OF INTEREST

The authors declare that there is no conflict of interest regarding the publication of this paper.

REFERENCES

[1] Soumbati, Y., Bouatou, I., Abushaban, A., Belmabkhout, Y., & Necibi, M. C. (2025). Review of membrane distillation for desalination applications: Advanced modeling, specific energy consumption, and water production cost. *Journal of Water Process Engineering, 71*, 107296.

[2] Teoh, G. H., Jawad, Z. A., Ooi, B. S., Chang, Y. S., & Low, S. C. (2022). Surface-templating of rough interface to efficiently recover aquaculture wastewater using membrane distillation. *Desalination, 522*, 115419.

[3] Shalaby, S. M., Kabeel, A. E., Abosheiasha, H. F., Elfakharany, M. K., El-Bialy, E., Shama, A., & Vidic, R. D. (2022). Membrane distillation driven by solar energy: A review. *Journal of Cleaner Production, 366*, 132949.

[4] Madupathi, M. M., Srishti, S., Fatima, S., & Sridhar, S. (2024). Sea and brackish water

desalination through a novel PVDF-PTFE composite hydrophobic membrane by vacuum membrane distillation. *Discover Chemical Engineering, 4*, 7.

[5] Zhou, L., Zhang, H., Ahmad, A. L., Tan, S. H., Low, S. C., & Li, C. (2023). Hierarchical structure design of electrospun membrane for enhanced membrane distillation treatment of shrimp aquaculture wastewater. *Separation and Purification Technology, 306*, 122591.

[6] Giraldo-Mejía, H., Quintero, Y. M., Mery, F., Rodriguez, F., Curcio, E., Estay, H., & Garcia, A. (2023). Plasma-grafting surface modifications to enhance membrane hydrophobicity for brine membrane distillation. *Desalination, 567*, 116942.

[7] Sheng, D., Li, X., Huang, X., Ma, D., Sun, C., Zhu, Y., Wang, X., Wang, Z., Feng, X., Zhao, S., & Wang, B. (2025). High-flux and anti-fouling membrane distillation membrane with VOC capture ability enabled by ZIF-8. *Nature Communications, 16*, 8021.

[8] Rosli, A., Ahmad, A. L., & Low, S. C. (2020). Enhancing membrane hydrophobicity using silica end-capped with organosilicon for CO_2 absorption in membrane contactor. *Separation and Purification Technology, 251*, 117429.

[9] Teoh, G. H., Jawad, Z. A., Khoerunnisa, F., & Low, S. C. (2025). Fouling dynamics and surface chemistry of superhydrophobic PVDF membranes for desalinating microalgae-rich hypersaline water. *Total Chemistry, 1*, 100005.

[10] Julian, H., Nurgirisia, N., Qiu, G., Ting, Y.-P., & Wenten, I. G. (2022). Membrane distillation for wastewater treatment: Current trends, challenges and prospects of dense membrane distillation. *Journal of Water Process Engineering, 46*, 102615.

[11] Wang, Y.-J., Liu, Y., Wei, X., Ding, L.-M., Feng, Y.-N., & Zhao, Z.-P. (2022). Polypropylene hollow fiber membrane prepared with green binary diluents via TIPS: Effects of spinning process parameters and VMD desalination performance. *Desalination, 541*, 116026.

[12] Bin Abid, M., Wahab, R. A., Salam, M. A., Moujdin, I. A., & Gzara, L. (2023). Desalination technologies, membrane distillation, and electrospinning: An overview. *Heliyon, 9*, e12810.

[13] Oleiwi, A. H., Jabur, A. R., & Alsalhy, Q. F. (2025). Electrospinning technology in water treatment applications: Review article. *Desalination and Water Treatment, 322*, 101175.

[14] Guo, X., Li, Y., Liu, Z., & Xiao, C. (2023). A new superhydrophobic polypropylene hollow fiber membrane preparation method and its application in treating high-salt brine. *Journal of Environmental Chemical Engineering, 11*, 109054.

[15] Janjhi, F. A., Chandio, I., Janwery, D., Vatanpour, V., & Castro-Muñoz, R. (2025). A review on hydrophobic electrospun nanofibers-based materials and membranes for water treatment: Challenges, outlook, and stability. *Separation and Purification Technology, 353*, 128370.

[16] Wang, X., Liang, Y., Pu, Z., He, J., & Yang, S. (2024). Transforming waste to treasure: Superhydrophobic coatings from recycled polypropylene for high-value application. *Progress in Organic Coatings, 188*, 108248.

[17] Teoh, G. H., Chin, J. Y., Ooi, B. S., Jawad, Z. A., Leow, H. T. L., & Low, S. C. (2020). Superhydrophobic membrane with hierarchically 3D-microtexture to treat saline water by membrane distillation. *Journal of Water Process Engineering, 37*, 101528.

[18] Fang, J., Zhang, L., Sutton, D., Wang, X., & Lin, T. (2012). Needleless melt-electrospinning of polypropylene nanofibres. *Journal of Nanomaterials, 2012*, 382639.

[19] Wang, J., Guo, J., Li, C., Yang, S., Wu, H., & Guo, S. (2014). Crystallization kinetics behavior and morphological evolution of polypropylene/poly(ethylene-co-octene) blends. *Journal of Polymer Research, 21*, 618.

[20] Chin, J. Y., Teoh, G. H., Ahmad, A. L., & Low, S. C. (2020). Superhydrophobic surface coating on electrospun polypropylene membrane to treat high-salinity water in membrane distillation. *Water Science and Technology, 82*, 2948–2961.

[21] Baig, M. I., Willott, J. D., & de Vos, W. M. (2020). Tuning the structure and performance of polyelectrolyte complexation based aqueous phase separation membranes. *Journal of Membrane Science, 615*, 118502.

[22] Li, J., Ren, L.-F., Shao, J., Tu, Y., Ma, Z., Lin, Y., & He, Y. (2020). Fabrication of triple-layer composite membrane and its application in membrane distillation. *Separation and Purification Technology, 234*, 116087.

[23] Ojedeji, D., & Doxastakis, M. (2024). Impact of chain orientation on the melting of the α-form of isotactic polypropylene. *Macromolecules, 57*, 8643–8655.

[24] Yang, J. (2010). Origin of double melting peaks of α-form isotactic polypropylene: Recrystallization and lamellar thickness hierarchy. *Journal of Applied Polymer Science, 118*, 1520–1526.

[25] Zhou, C., Hou, Z., Lu, X., Liu, Z., Bian, X., Shi, L., & Li, L. (2010). Effect of polyethersulfone molecular weight on structure and performance of ultrafiltration membranes. *Industrial & Engineering Chemistry Research, 49*, 9988–9997.

[26] Chang, P. T., Baharuddin, I. M., Ng, Q. H., Teoh, G. H., Ahmad, A. L., & Low, S. C. (2022). Creating membrane–air–liquid interface through a rough hierarchy structure for membrane gas absorption to remove CO_2. *International Journal of Energy Research, 46*, 5067–5082.

[27] Ahmad, A. L., Chin, J. Y., Mohd Harun, M. H. Z., & Low, S. C. (2022). Environmental impacts and imperative technologies for sustainable aquaculture wastewater treatment: A review. *Journal of Water Process Engineering, 46*, 102553.

[28] Krivorot, M., Kushmaro, A., Oren, Y., & Gilron, J. (2011). Factors affecting biofilm formation and biofouling in membrane distillation of seawater. *Journal of Membrane Science, 376*, 15–24.

[29] Gao, B., Liu, Z., Tan, S. H., & Low, S. C. (2025). Addressing critical challenges of biofouling

in solar evaporation: Advanced strategies for anti-biofouling performance. *Separation and Purification Technology, 367*, 132874.

[30] Xie, M., & Gray, S. R. (2017). Silica scaling in forward osmosis: From solution to membrane interface. *Water Research, 108*, 232–239.

[31] Teoh, G. H., Jawad, Z. A., Chan, D. J. C., & Low, S. C. (2023). Surface regeneration of templated PVDF membrane for microalgae-rich high-saline wastewater treatment in membrane distillation. *Desalination, 565*, 116858.

[32] He, F., Sirkar, K. K., & Gilron, J. (2009). Studies on scaling of membranes in desalination by direct contact membrane distillation: $CaCO_3$ and $CaSO_4$ systems. *Chemical Engineering Science, 64*, 1844–1859.

[33] Warsinger, D. M., Swaminathan, J., Guillen-Burrieza, E., Arafat, H. A., & Lienhard, J. H. V. (2015). Scaling and fouling in membrane distillation for desalination applications: A review. *Desalination, 356*, 294–313.

[34] Sheikholeslami, R., & Ng, M. (2001). Calcium sulfate precipitation in presence of calcium carbonate: Thermodynamics and kinetics. *Industrial & Engineering Chemistry Research, 40*, 3570–3578.

[35] Salvador Cob, S., Beaupin, C., Hofs, B., Nederlof, M. M., Harmsen, D. J. H., Cornelissen, E. R., Zwijnenburg, A., Genceli Güner, F. E., & Witkamp, G. J. (2012). Silica and silicate precipitation as limiting factors in high-recovery reverse osmosis operations. *Journal of Membrane Science, 423–424*, 1–10.

[36] Tong, T., Liu, X., Li, T., Park, S., & Anger, B. (2023). A tale of two foulants: The coupling of organic fouling and mineral scaling in membrane desalination. *Environmental Science & Technology, 57*, 7129–7149.